Supporting Information

to the article

Conical lipids in flat bilayers induce packing defects similar to that induced by positive curvature

Lydie Vamparys[1,2,3], Romain Gautier[4], Stefano Vanni[4], W.F. Drew Bennett[5], D. Peter Tieleman[5], Bruno Antonny[4], Catherine Etchebest[1,2,3], and Patrick F.J. Fuchs[1,2,3]

[1]INSERM, U665, F-75739 Paris, France

[2]Univ Paris Diderot, Sorbonne Paris Cité, UMR_S 665, F-75739 Paris, France

[3]Institut National de la Transfusion Sanguine, F-75739 Paris, France

[4]IPMC, UMR 7275 CNRS, Université de Nice Sophia Antipolis, F-06560, Valbonne, France

[5]Department of Biological Sciences, and Institute for Biocomplexity and Informatics, University of Calgary, Calgary, Alberta, Canada

Supplementary Methods

Bilayers of different sizes were simulated for different times according to the type of analysis. The choice was motivated by the best balance between convergence of the measured property / computational cost / avoidance of issues due to undulations on big patches. To evaluate the error, we generally divided the trajectory in different numbers of blocks and calculated the standard deviation of the mean of each block (as summarized in Table S1).

Hydrophobic thickness

Hydrophobic thickness was evaluated from the peak to peak distance of C2 atoms in density plots (see Figure 2c of the main paper, dashed vertical lines).

Area and volume of DOPC and DOG

The area of DOPC and DOG was evaluated by analyzing simulations of 70 lipids at different DOG fraction, as proposed by Edholm and Nagle (1). A similar analysis was performed to assess the volume of DOPC and DOG (see Figures S1 and S2 below).

Lateral diffusion

Lateral diffusion of DOPC molecules (considering phosphorous atoms of DOPC) was calculated on patches of 128 lipids from the slope of the mean square displacement curve using Einstein law. To correct for the overall motion of each monolayer, the linear momentum was removed at each step for each monolayer separately (2). The trajectory was divided into two blocks. The error was evaluated by calculating the standard deviation over the two leaflets of the two blocks.

Potential of mean force

Using a procedure similar to ref (3) (note that the force field therein is slightly different to the one used in the present study), we used umbrella sampling to determine the potential of mean force (PMF) for moving a DOG (or DOPC) head group from equilibrium into the center of the bilayer. A harmonic potential was applied to the OH of DOG (or phosphate of DOPC) with respect to the center of mass of the bilayer, with a force constant of 3000 kJ mol^{-1} nm^{-2}. For the DOG and DOPC PMF, 21 independent simulations with a 0.1 nm spacing between the umbrella positions (0 nm to 2 nm), were run for 120 ns (two sets with 60 ns for each of the 21 umbrella windows). The starting conformations of the two sets were obtained by pulling either DOG or DOPC in the two directions. The weighted histogram analysis method was used to calculate the PMFs (4). We thus obtained one PMF for each leaflet and the error was estimated as the standard deviation over the two leaflets.

Lateral pressure profile

The lateral pressure profile was computed on the patches of 128 lipids as a post-trajectory analysis using a modified version of GROMACS 4.0.2 (5, 6). The simulation box was

basically cut into slices of 0.1 nm along the z direction, and the local pressure was computed for each slice from the local virial as described in refs (5, 6). The local pressure profile is evaluated as follows:

$$\pi(z) = P_L - P_N \qquad (1),$$

where P_L is the lateral component (in the xy plane, $P_L=(P_{xx}+P_{yy})/2$) of the pressure, and P_N is the normal component (along z, $P_N=P_{zz}$). Recently Ollila noticed that all-atom simulations give non-constant P_N as compared to coarse-grained simulations for which sampling is more than two orders of magnitude higher (7). According to this author, one possible explanation could be that the rerun is performed using a long cutoff (2.0 nm) for computing electrostatics, whereas the original simulation runs are performed using PME (the use of a cutoff is due to the difficulty of extracting specific contributions from the reciprocal term of PME). In our simulations, P_N was not constant over z but similar in all simulations. As we are only interested in the relative behavior between the different systems, we thus only report the P_L component in the presented pressure profiles that we call $P(z)$, as was done previously (5, 6). When $P(z)$ is positive, the bilayer tends to expand whereas when $P(z)$ is negative it tends to shrink. For a bilayer with no spontaneous curvature, the integral of $P(z)$ (*i.e.* surface tension γ) should be equal to 0 (perfect balance between negative and positive contributions).

Bilayer compressibility

The area compressibility modulus K_A is evaluated from the fluctuations of bilayer area:

$$K_A = (Ak_BT)/\sigma^2_A \qquad (2),$$

where A is the total bilayer area, k_B the Boltzmann constant, T the absolute temperature and σ^2_A the variance of A. To avoid issues related to undulations we used small patches of 70 lipids (almost undulation free) but pushed the simulations up to 800 ns to evaluate the error (by dividing the trajectory in 3 slices - after 100 ns of equilibration – and computed the standard deviation of K_A over the 3 slices). It has been shown that computing compressibility on small patches overestimates the K_A value (7), and on big patches the undulations have to be taken out of the pure area fluctuations (7). Nevertheless we were only interested in the trend on going from a system to another, not in the precise reproduction of experimental values.

Bending rigidity

Bilayer rigidity was evaluated from the undulations of the big patches (1,024 lipids). Using the continuum model of Helfrich (8), it is possible to extract the rigidity (or bending) modulus κ from the power spectrum (see for example refs (9, 10)):

$$\left\langle \left| U(q) \right|^2 \right\rangle = k_B T / A\kappa q^4 \qquad (3),$$

where A is the total area of the system, $U(q)$ is the discrete Fourier transform of the out-of-plane displacement $u(\mathbf{r})$ of the bilayer surface in Monge representation ($\mathbf{r}=[r_x,r_y]$), and <…> means averaging over the trajectory (note that the term in q^{-2} involving microscopic surface tension γ has been omitted since we are only interested in the undulation regime). To get κ from equation (3), we first had to evaluate $U(q)$. To do so, we first discretized the squared bilayer of edge length L into an $N\times N$ mesh of elementary grid size $l=L/(N-1)$. The phosphorous atom of the upper leaflet with the lowest [x,y] coordinates was chosen arbitrarily as the origin (*i.e.* $\mathbf{r}_1$). For each grid point k and for each leaflet, we computed $z(\mathbf{r}_k)$ as the mean of the z coordinate of the three nearest phosphorous atoms. The out-of-plane displacement was computed from the mean z position between the two leaflets: $u(\mathbf{r}_k)=½(z_{upper}(\mathbf{r}_k)+z_{lower}(\mathbf{r}_k))$. $U(\mathbf{q})$ was then evaluated from $u(\mathbf{r}_k)$ using a 2D discrete Fourier transform:

$$U(\mathbf{q}) = \frac{1}{N^2}\sum_{k=1}^{N^2} u(\mathbf{r}_k) e^{-i\mathbf{q}.\mathbf{r}_k} \qquad (4),$$

where $\mathbf{q}$ is the 2D wave vector, *i.e.* $\mathbf{q}=[q_x,q_y]=2\pi[n_x,n_y]/L$ (n_x and n_y are integers spanning 0 to N-1). Finally, $U(\mathbf{q})$ was converted to $U(q)$, where q is the norm of $\mathbf{q}$.

κ has been evaluated from formula (3) using a non-linear fit (so that it enforces the q^{-4} behavior, *i.e.* a slope of -4 from the plot $|U(q)|^2$ vs q with a log-log scale). Note that we used only the points between 0.33 (the lowest point due to the size of our system, *e.g.* roughly 19x19 nm for the pure DOPC system) and 1 nm^{-1} which correspond to the undulation regime.

For this analysis, we used one frame every 100 ps from 5 ns to 200 ns. Error was evaluated by dividing the trajectory in 3 blocks and by computing the corresponding standard deviation.

Packing defect mapping

Packing defects were mapped from simulations of 280 lipids, taking one frame per 100 ps from 100 to 200 ns. For each frame, water and ions were taken out and the corresponding pdb file was used in a pipeline of scripts to extract the packing defect areas. The next two sections describe the pipelines used for the ASA method and our new Cartesian methods.

Packing defect mapping using 1) the ASA approach

This method has been introduced recently by Voth and coworkers (11). We used the same global framework but with different details. Starting from the structure of the bilayer without water and ions, we duplicated the system in all *xy* directions to avoid issues on the edges. The lipids 1.5 nm away from the central patch were discarded. We then computed the accessible surface area (ASA) with the program NACCESS (12) using the same van der Waals radii as in ref (11). In order to compare our results to this work, we used the same probe radius (0.3 nm). This size was initially chosen because it roughly corresponds to the volume of a big hydrophobic residue such as Phe. All aliphatic carbons from the central (initial) patch with a non-null ASA were then extracted and analyzed for each leaflet separately. All non-null ASA were considered as packing defects and projected on the *xy* plane and converted to defect radii located at the (*x*,*y*) position of the corresponding atom (at this stage, a defect is thus a circle). A distance matrix was then computed between all individual defects, and overlapping defects were merged in a single defect according to the following criterions: i) if two defects overlapped (distance from their center < sum of their radii) they were merged into a single one; ii) if two defects did not overlap but were separated by a distance shorter than a threshold (distance from their center < sum of their radii + threshold), the defects were merged. We chose a threshold of 0.3 nm based on visual inspection of several snapshots (so that no polar atom could be located between the two defects). The area of merged defects was then computed using a grid approach with elementary squares of 0.01 nm^2.

Packing defect mapping using 2) the Cartesian scheme

We selected a plane that is perpendicular to the membrane normal and created a grid of 0.1 nm resolution. For each grid point, we scanned the normal to the membrane plane starting from the solvent and descending up to 0.1 nm below the nearest glycerol (C2 carbon of *sn*-2 chain). In the following, we ignore solvent and ion atoms and the analysis on each leaflet is done separately. At each *z* position of a given grid point, the presence of an eventual

overlapping atom was evaluated by calculating a 3D distance between the grid point center and the center of any atom of the bilayer. Overlap was assigned when this distance was shorter than the grid point diagonal half-length (0.07 nm) plus the van der Waals radius of the atom (see Figure S1). If a polar head atom was encountered the grid point was discarded. If an aliphatic atom was met, we retained the grid point and defined it as a chemical defect of size 0.01 nm^2. If the first atom met was aliphatic and its *z* position was 0.1 nm below the *sn*-2 carbon of the nearest glycerol, the grid point was assigned as a geometrical defect of size 0.01 nm^2. Adjacent elementary defects were then merged, resulting in defects of various sizes. Note that geometrical defects represent a sub-category of chemical defects. The van der Waals radii used for this analysis were taken from the r_{min} values (distance at which the Lennard-Jones is minimal) of the Berger united-atom force field (13) (after the initial observation that classical radii used to compute ASA in NACCESS (12) or VMD (14) were giving poorly discriminated results and to better take into account the relative size of CH_2 and CH_3).

Sensitivity of packing defect size distributions to different parameters

We first checked whether the distributions were sensitive to system size. Too small patches (notably 70 lipids) gave in general distributions shifted to the left. We found that patches of 280 lipids were giving results close to those obtained on patches of 1,024 lipids. We thus performed all the packing defect analyses on systems of 280 lipids.

For the ASA method, the results depended on the chosen threshold used for merging defects. We used a threshold of 0.3 nm. A smaller threshold gives distributions shifted to the left and vice-versa. We found that the value of 0.3 nm was the best compromise by visual inspection of various snapshots (two defects should be merged if and only if there is no polar head atom in between).

For each distribution in Figure 5 of the main paper, we carefully checked their proper convergence. We found that 1,000 frames (from 100 to 200 ns every 100 ps) were giving enough statistics (*e.g.* for DMPC the number of defects was 51,149 for the ASA method, 107,744 for chemical defects, and 65,721 for geometrical defects; for DOPC/DOG the number of defects was 71,972 for the ASA method, 109,695 for chemical defects, and 83,423 for geometrical defects).

The distributions were also sensitive to the way of binning the corresponding histogram from the raw data. For each method (ASA, chemical or geometrical defects), we imposed (for each

lipid composition) 101 breaks to get 100 distinct bins (from 0 to 1.2 nm for ASA and geometrical defects, and from 0 to 2.5 nm for chemical defects).

We also tested the effect of removing ions. Note that all the patches of 280 lipids used for studying packing defects in the main paper were simulated with 120 mM of ions (Na^+ / Cl^-). Some additional simulations without ions were thus performed. Removing ions marginally affected the decays and did not change the relative differences between compositions.

Last, we tested the effect of temperature. Increasing temperature shifted the distributions to the right (towards larger defects), but again the relative difference between compositions was preserved. The increase of temperature for a particular composition can thus mimic the distribution of another composition at a different temperature (for example DMPC at 333K displays the same distribution as DOPC at 300K). This parameter is important since we performed simulations at a higher temperature (333K) in the accompanying paper.

Supplementary Figures

Figure S1. Scheme of the Cartesian method for detecting packing defects. First a grid with 0.1 nm resolution (in light blue above the bilayer in surface representation) is built and the analysis is done separately on each leaflet (note that the size of each grid point has been scaled up for clarity). For each grid point, the z position is scanned starting outside the bilayer and descending towards the bilayer center. At each z position, the method searches an eventual overlap with any atom of that leaflet. A distance d between the center of the grid point and the center of each atom is calculated. An overlap is assigned when d is shorter than the van der Waals radius (r_{vdw}) plus the grid point half diagonal length ($ldiag_{1/2}$). The two possible cases are sketched in top view on the left of the figure (the grid point is represented as a light blue square whereas the atom is represented as a black circle): 1) no overlap is assigned ($d > r_{vdw} + ldiag_{1/2}$); 2) an overlap is assigned when the atom spans the inscribed or circumscribed circle of the grid point ($d < r_{vdw} + ldiag_{1/2}$). The snapshot in surface representation was generated using Pymol (15).

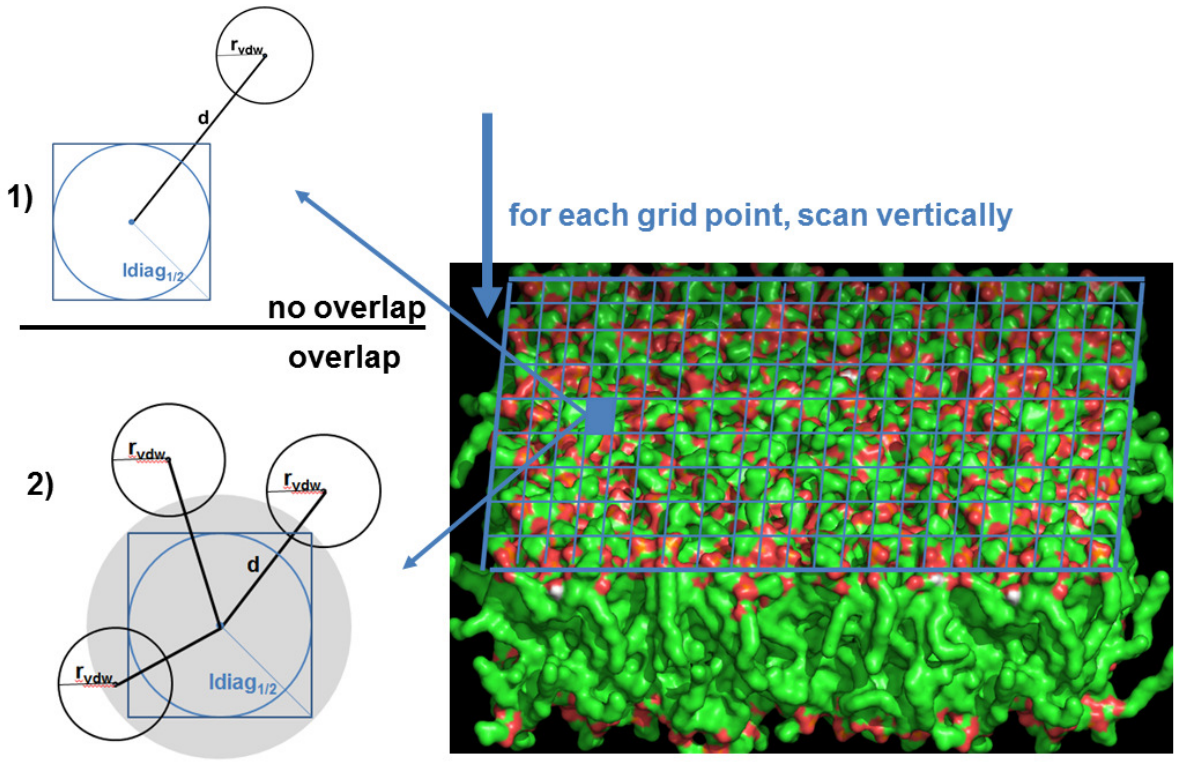

Figure S2. Evaluation of DOPC and DOG area from the simulations at different DOPC/DOG ratios. These areas were extracted from a linear fit to the following equation: $\frac{A_{\mathrm{L}}(x)}{1\text{-}x} = A_{\mathrm{DOPC}}(x) + \frac{x}{1-x} A_{\mathrm{DOG}}(x)$, where A_{L} is the area per total lipid, A_{DOPC} the area per DOPC, A_{DOG} the area per DOG, x the mol fraction of DOG (1). DOPC area thus corresponds to the intercept and that of DOG to the slope. We find A_{DOPC}=0.70 nm^2 and A_{DOG}=0.46 nm^2.

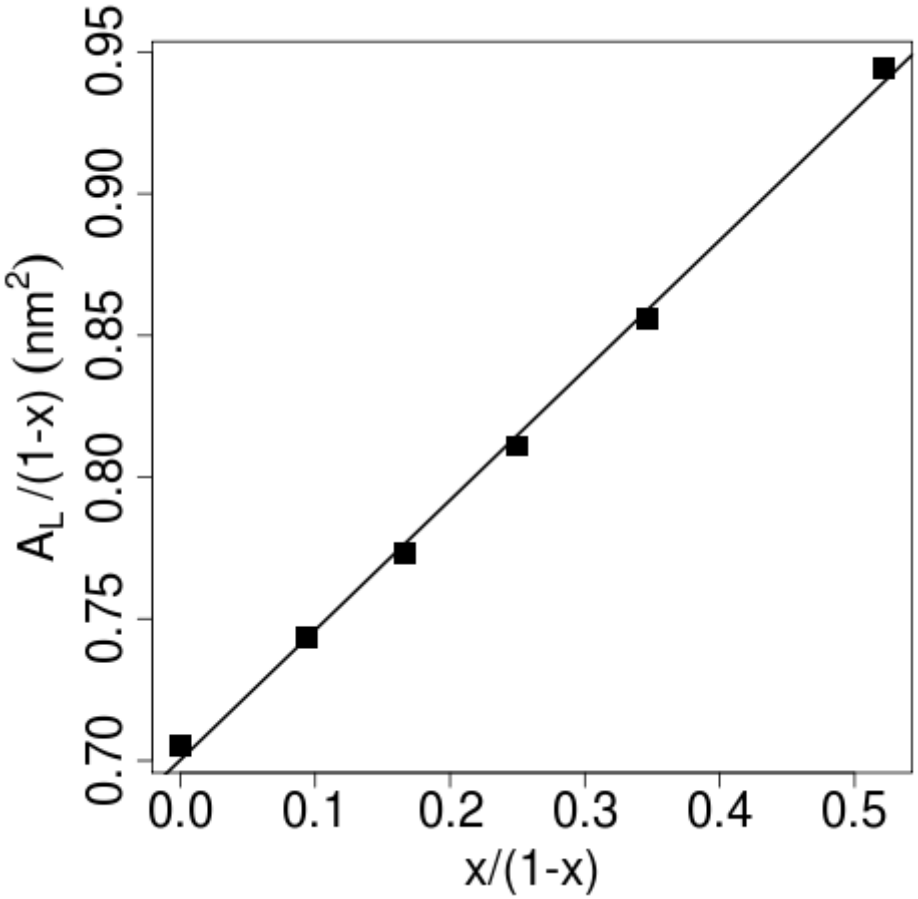

Figure S3. Evaluation of DOPC and DOG volume from the simulations at different DOPC/DOG ratios. These volumes were extracted from a linear fit to the following equation: $V_L(x)=(1-x)V_{DOPC}(x)+xV_{DOG}(x)$, where V_L is the volume per total lipid, V_{DOPC} the volume per DOPC, V_{DOG} the volume per DOG, x the mol fraction of DOG (1). V_L required an additional simulation of pure water (same number of molecules as for the bilayer systems) and was computed as follows: $V_L=(V_{bilayer\_system}-V_{water})/N$, where N is the total number of lipids, V_{water} is the volume of the water box, $V_{bilayer\_system}$ is the volume of the whole system containing the bilayer (bilayer+water). V_{DOPC} was computed from the simulation at x=0 and V_{DOG} was extrapolated from the straight line at x=1. We find V_{DOPC}=1.31 nm^3 and V_{DOG}=1.12 nm^3.

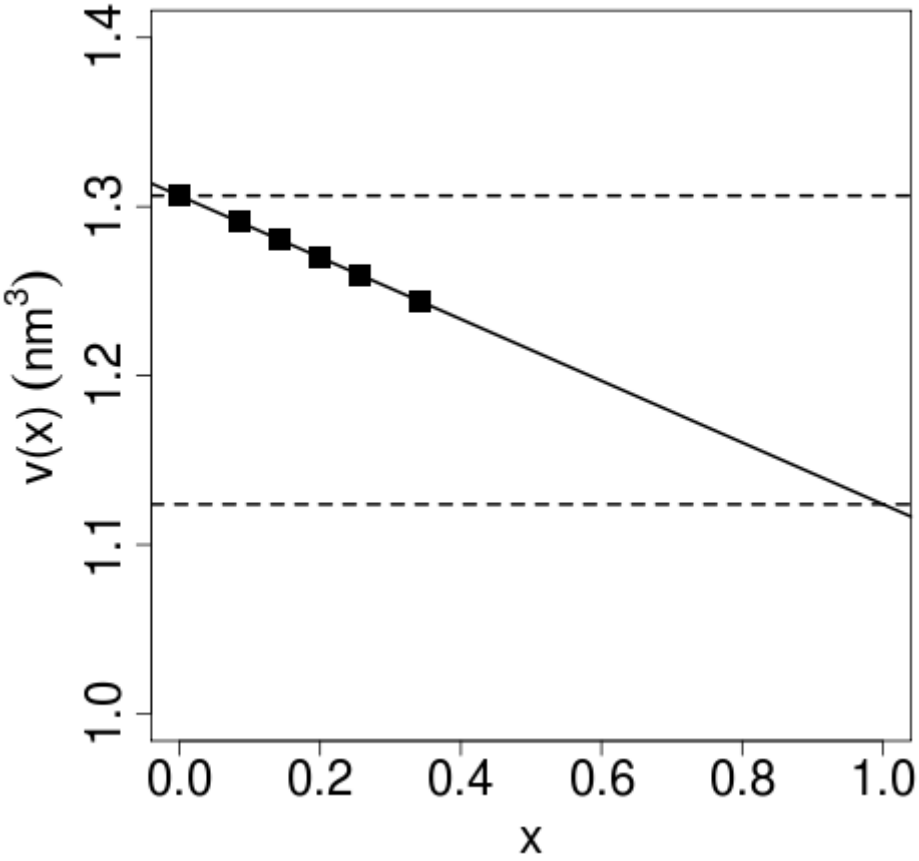

Figure S4. Radial distribution function $g(r)$ of oxygen atoms O4 vs water oxygen atoms OW. O4 atom corresponds to the oxygen that is connecting the glycerol and the phosphate group in DOPC, whereas it is the oxygen of the hydroxyl group in DOG (see Figure 1 of the main article). The top panel shows any O4 atom for both systems. In the bottom panel, the detail is given for DOG and DOPC in the DOPC/DOG mixture. The hydrogen-bond donor and acceptor capacity of O4 in DOG explains that the first peak is higher in DOPC/DOG (red) compared to pure DOPC (black) for which O4 is only acceptor. Inversely, the second peak is lower in DOPC/DOG because DOG is partitioned deeper towards the bilayer center and has thus less second-neighbor OW atoms accessible.

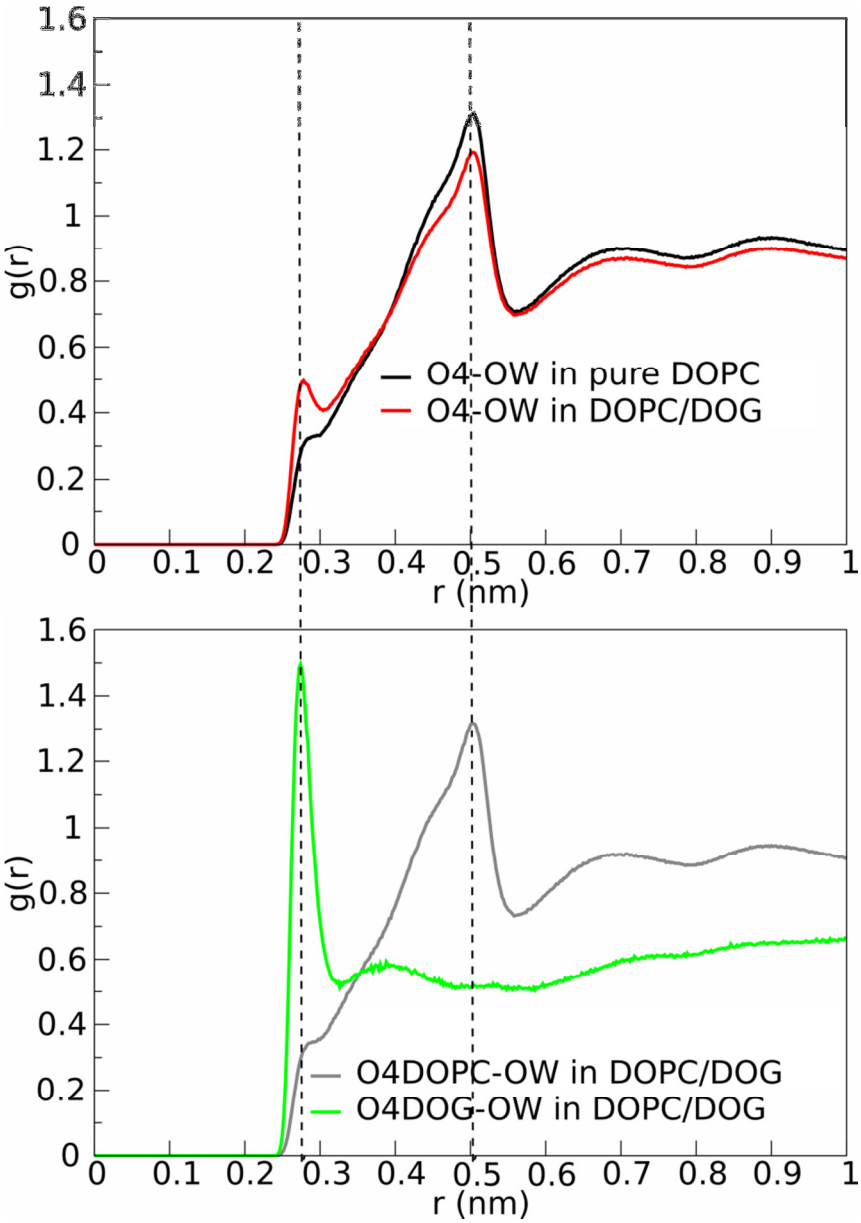

Figure S5. Snapshots during DOG and DOPC flip-flop. Water: thick blue lines; DOPC: thin grey lines; DOG: thin red lines; DOPC nitrogen: grey balls; DOG hydroxyl: red balls. The restrained lipid is shown in thicker lines. A and B. DOG flip-flop across a pure DOPC bilayer. C and D. DOPC flip-flop across a pure DOPC bilayer. For A and C, the restrained lipids head group is at the bilayer center, and at 0.6 nm from the bilayer center of B and D. The DOG in the center of the bilayer (A) loses its hydration whereas there is a persisting water pore for DOPC (C). The snapshots were generated with VMD (14).

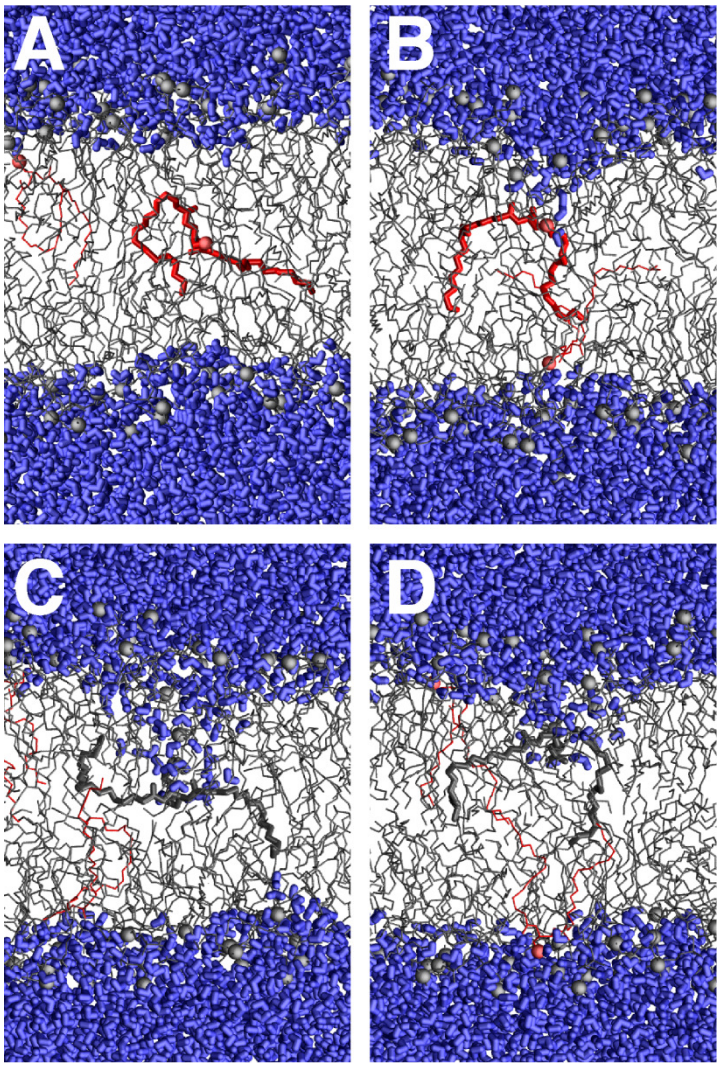

Figure S6. Distribution of the fraction of area occupied by packing defects within the total DOG/DOPC area for (A) geometric and (B) chemical defects. The mean and standard deviation are reported in Table 2 of the main manuscript. The vertical dotted lines represent the mean of each distribution. These distributions were accumulated from the trajectory of 280 lipids on 3000 snapshots (one every 100 ps).

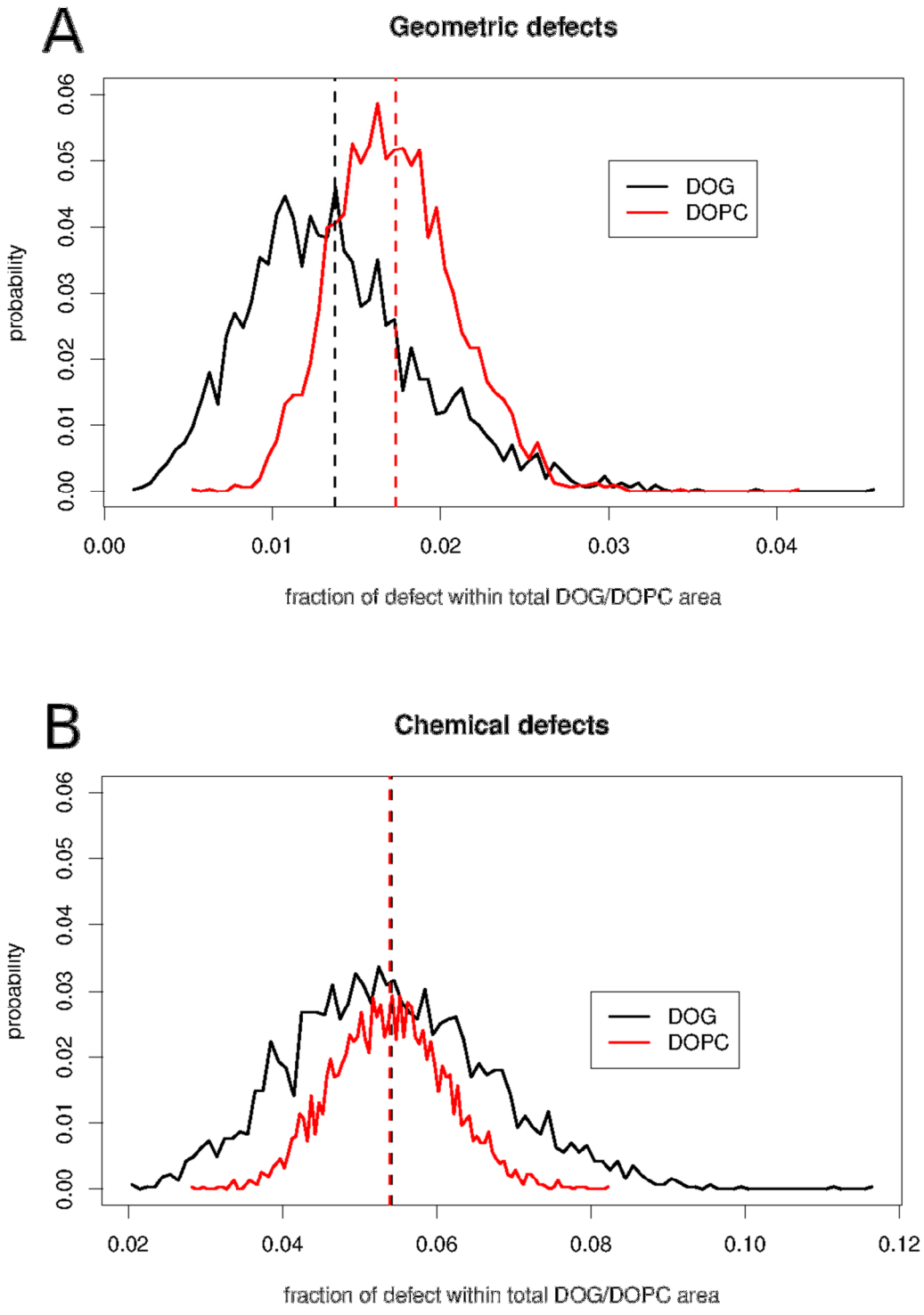

Figure S7. Packing defects do not co-localize with DOG. The snapshot has been taken from a simulation of a DOPC/DOG membrane (280 lipids). The aliphatic chains of DOG and DOPC are represented in blue and pale-green spheres, respectively (for clarity no polar head is shown). Packing defects are depicted as magenta spheres (one per grid point). One can clearly see that the defects are located either on DOG or DOPC, and that there is no specific preference of packing defects for DOG. Similar analysis on several snapshots leads to the same conclusion. This snapshot was rendered with Pymol (15).

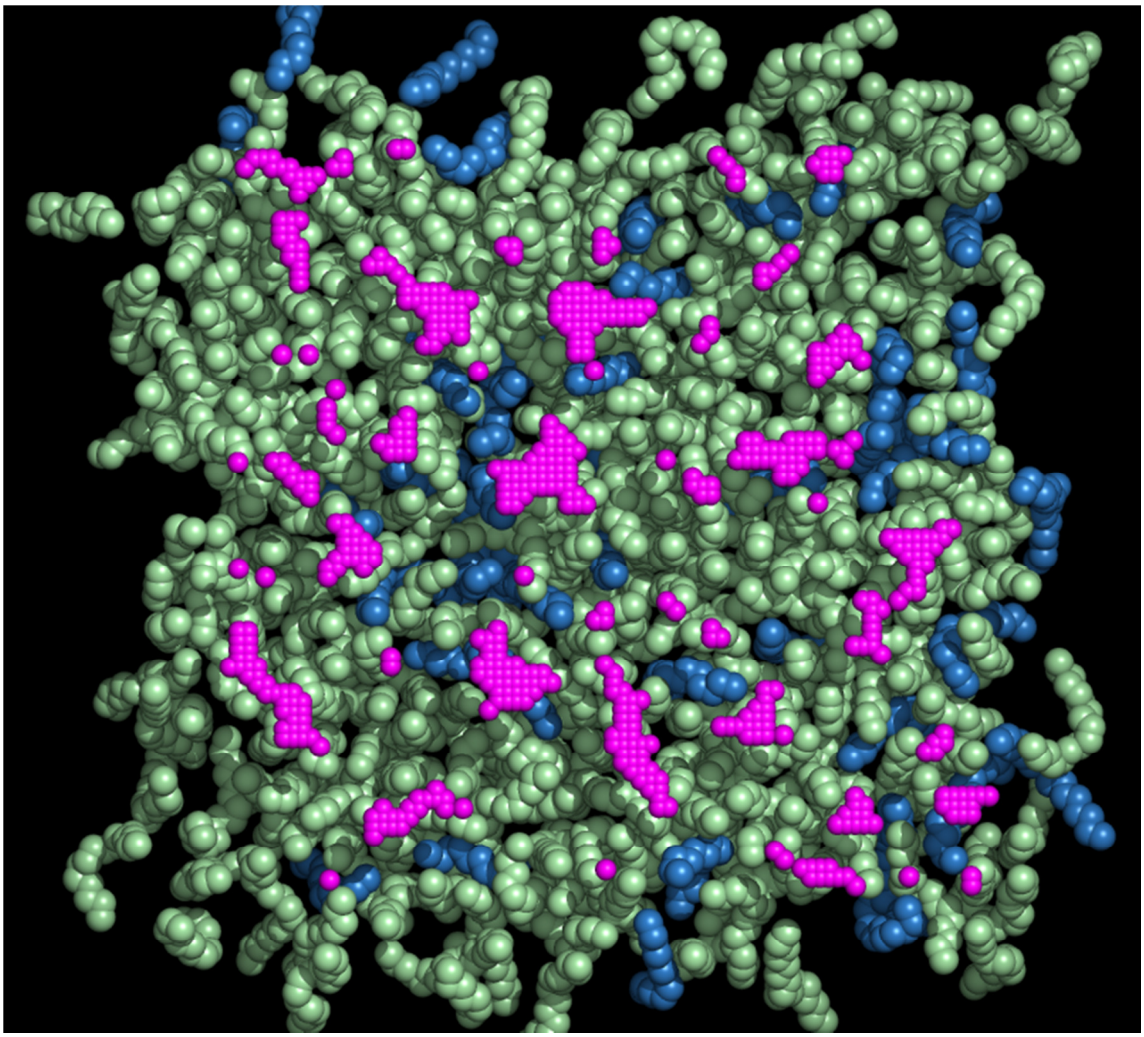

Table S1. Overview of the different simulations and type of analysis. The first column indicates the lipid composition, the second the patch size, the third the simulation time used for the analysis (after equilibration), the fourth the number of blocks used for calculating the error (as the standard deviation of the mean of each block), the last column indicates the type of analysis.

System	Nb lipids	Time (ns)	Nb blocks	Type of analysis
Pure DOPC DOPC-10%DOG DOPC-15%DOG DOPC-20%DOG DOPC-25%DOG DOPC-35%DOG	70	100-200	1	Area/lipid Volume/lipid
Pure DOPC DOPC-15%DOG	70	100-200	3	Hydrophobic thickness
pure DOPC DOPC-15%DOG	70	100-800	3	Compressibility modulus
pure DOPC DOPC-15%DOG	128	100-300	1	Density Radial distribution
pure DOPC DOPC-15%DOG	128	100-300	3	Lateral pressure profile
pure DOPC DOPC-15%DOG	128	100-300	2	Lateral diffusion
pure POPC pure DMPC pure DOPC DOPC-15%DOG	280	100-200	1	Packing defects
pure DOPC DOPC-15%DOG	1024	5-200	3	Bending rigidity modulus

Supporting References

1. Edholm, O., and J. F. Nagle. 2005. Areas of Molecules in Membranes Consisting of Mixtures. Biophys J 89:1827-1832.
2. Wohlert, J., and O. Edholm. 2006. Dynamics in atomistic simulations of phospholipid membranes: Nuclear magnetic resonance relaxation rates and lateral diffusion. J Chem Phys 125:204703.
3. Bennett, W. F. D., and D. P. Tieleman. 2012. Molecular simulation of rapid translocation of cholesterol, diacylglycerol, and ceramide in model raft and nonraft membranes. J Lipid Res 53:421-429.
4. Kumar, S., J. M. Rosenberg, D. Bouzida, R. H. Swendsen, and P. A. Kollman. 1992. The weighted histogram analysis method for free-energy calculations on biomolecules. I. The method. J Comput Chem 13:1011-1021.
5. Ollila, O. H. S., H. J. Risselada, M. Louhivuori, E. Lindahl, I. Vattulainen, and S. J. Marrink. 2009. 3D Pressure Field in Lipid Membranes and Membrane-Protein Complexes. Phys Rev Lett 102:078101.
6. Ollila, S., M. T. Hyvönen, and I. Vattulainen. 2007. Polyunsaturation in Lipid Membranes: Dynamic Properties and Lateral Pressure Profiles. J Phys Chem B 111:3139-3150.
7. Waheed, Q., and O. Edholm. 2009. Undulation Contributions to the Area Compressibility in Lipid Bilayer Simulations. Biophys J 97:2754-2760.
8. Helfrich, W. 1973. Elastic properties of lipid bilayers: theory and possible experiments. Z Naturforsch C 28:693–703.
9. Brandt, Erik G., Anthony R. Braun, Jonathan N. Sachs, John F. Nagle, and O. Edholm. 2011. Interpretation of Fluctuation Spectra in Lipid Bilayer Simulations. Biophys J 100:2104-2111.
10. Lindahl, E., and O. Edholm. 2000. Mesoscopic Undulations and Thickness Fluctuations in Lipid Bilayers from Molecular Dynamics Simulations. Biophys J 79:426-433.
11. Cui, H., E. Lyman, and G. A. Voth. 2011. Mechanism of Membrane Curvature Sensing by Amphipathic Helix Containing Proteins. Biophys J 100:1271-1279.
12. Hubbard, S. J., and J. M. Thornton. 1993. NACCESS. Department of Biochemistry and Molecular Biology, University College London.
13. Berger, O., O. Edholm, and F. Jahnig. 1997. Molecular dynamics simulations of a fluid bilayer of dipalmitoylphosphatidylcholine at full hydration, constant pressure, and constant temperature. Biophys J 72:2002-2013.
14. Humphrey, W., A. Dalke, and K. Schulten. 1996. VMD: visual molecular dynamics. Journal of molecular graphics 14:33-38, 27-38.
15. Schrodinger, L. 2010. The PyMOL Molecular Graphics System, Version 1.3r1.